Published version at http://dx.doi.org/10.1088/0957-0233/18/5/026

Dielectric Metrology with Coaxial Sensors

A P Gregory and R N Clarke
Enabling Metrology Division, National Physical Laboratory.
Hampton Road, Teddington
Middlesex, TW11 0LW
United Kingdom

Coaxial sensors are used in applications that require accurate and traceable measurements of complex permittivity. For example, coaxial sensors are often used for measurement of the complex permittivity of tissue Equivalent Materials (TEMs) used in Specific Absorption Rate (SAR) measurements of exposure to RF fields. It is therefore important that well-founded metrological techniques for their use are developed and published. Although there are many published papers on coaxial sensors, few discuss the experimental techniques required to obtain the most accurate results. In this paper experimental approaches for obtaining the most accurate measurements are described. Common pitfalls with the technique are discussed. A Monte-Carlo Modelling (MCM) technique is used to provide estimates of uncertainty which are compared to those of measurements on reference liquids made with 3.5-mm, 7-mm and 15.1-mm diameter sensors. The MCM technique allows uncertainties to be estimated when measuring dielectrics for which there are no reference materials that have comparable properties, for example for TEMs at frequencies below 100 MHz.

Keywords: Dielectric measurement, microwave measurement, open-ended coaxial probe, Vector Network Analyser measurements, Specific Absorption Rate measurement

1. INTRODUCTION

Coaxial sensors are used for measuring the complex permittivity of lossy materials at RF and microwave frequencies. They are also referred to as *coaxial probes*, *coaxial-line probes*, and *open-ended coaxial-line*s. They are used in conjunction with reflectometers such as Vector Network Analysers (VNAs) that measure complex reflection coefficient of travelling waves in transmission lines. From these measurements the complex permittivity of samples can be computed at each measurement frequency.

The aims of this paper are (i) to show how coaxial sensor measurements can be made traceable to international standards, (ii) to describe methods for obtaining best measurement accuracy, and (iii) to propose a method for assessing their uncertainties by using *Monte Carlo Modelling* (MCM). Much of the information that is given here is not available from a single source. Traceable measurements with quantified measurement uncertainty are essential for a number of the applications for which coaxial sensors are currently used. They include measurements on Tissue Equivalent Materials (TEMs) used in Specific Absorption Rate (SAR) determinations, for which traceable measurements with known uncertainty are required by the international standards [1][2][3].

In Section 2 we present a short overview of the coaxial sensor method, placing particular emphasis on issues that relate to measurement accuracy. In Section 3, dielectric reference liquids for calibration and checking are discussed. Section 4 presents a least-squares method for calibrating coaxial sensors, which can provide valuable information on measurement accuracy. Section 5 covers practical issues of calibration and measurement while Section 6 describes the application of the MCM technique for estimating the uncertainties of coaxial sensor measurements. Section 7 describes experiments in which reference liquids are measured to demonstrate the levels of accuracy that can be achieved, and compares this data with the MCM estimates of uncertainty. The findings are summarised in the Conclusion, Section 8.

We will primarily be concerned here with measurements on lossy samples of liquids, or else on malleable solids that make good contact with the working face of the sensor, without any gaps. Techniques for measurement of hard materials using coaxial sensors are described elsewhere, e.g. in [4]. A recent review [5] by the present authors covers a wider range of measurement techniques and places coaxial sensor measurements on lossy liquids in a broader metrological context.

The following symbols are used in this paper: $\varepsilon^* = \varepsilon' - j\varepsilon''$ is the *complex relative permittivity* of a material and $\tan\delta = \varepsilon''/\varepsilon'$ is its *loss tangent.* Instead of ε'', *conductivity* is often quoted. It is given by $\sigma = \varepsilon'' \cdot \varepsilon_o \cdot 2\pi f$ S/m where the permittivity of free space $\varepsilon_o = 8.854 \cdot 10^{-12}$ F/m.

2. COAXIAL SENSORS

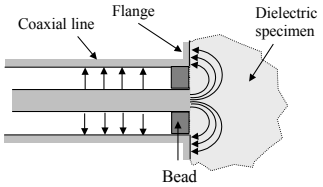

Figure 1: Schematic diagram of a coaxial sensor. Electric fields are represented by the arrowed lines.

A typical coaxial sensor is shown in Figure 1. It consists

Published version at http://dx.doi.org/10.1088/0957-0233/18/5/026

of a truncated coaxial line with a flanged end. Flange-less designs (which are often referred to as "probes") are also used, particularly in smaller line sizes. The results presented in this paper were obtained using flanged sensors only. A dielectric insert (known as a "bead") prevents the ingress of samples. The sensitivity of coaxial sensors varies considerably with (i) frequency, (ii) the complex permittivity of the sample and (iii) the dimensions of the sensor. The optimum diameter of sensors falls with increasing measurement frequency. Coaxial sensors are normally used at frequencies below the cut-off frequency for the TE_{11} mode in the bead [6], i.e. so that only the TEM mode propagates. Figure 2 shows a mapping of complex permittivity (ε' and ε'') onto the complex reflection coefficient (S_{11}) plane. Such mappings provide a visual representation of how S_{11} varies with ε' and ε'' at a fixed frequency and give an indication of measurement sensitivity. They are a useful aid for choosing the most appropriate size of sensor for a particular measurement. The coaxial sensors used in the work presented here are shown in Figure 3.

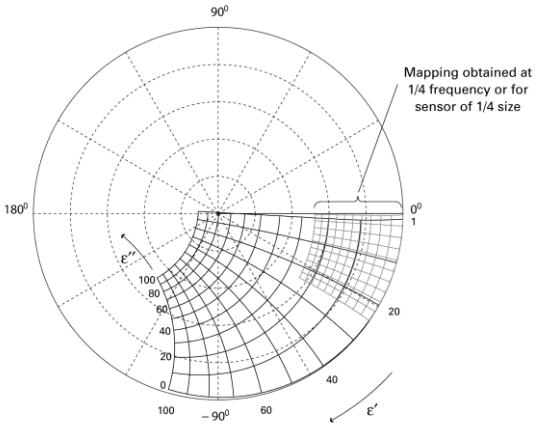

Figure 2. A mapping of sample complex permittivity, $\varepsilon^* = \varepsilon' - j\varepsilon''$, onto the complex reflection coefficient (S_{11}) plane for a coaxial sensor with bead permittivity 2.54, O.D. 15.1 mm, I.D. 4.0 mm at 0.5GHz. At one quarter of this frequency, or when using a sensor with linear dimensions that are four times smaller, the mapping can be seen to fill a smaller area. As frequency is reduced S_{11} tends to move towards the point $(+1 + j0)$ and becomes less sensitive to the complex permittivity of the sample.

In the sensor design of Figure 1, in which the inner and outer conductor diameters in both the air-dielectric coaxial line and in the bead region are identical, there is an impedance mismatch at the air-dielectric/bead-dielectric interface, which itself produces a signal reflection. While the VNA software calibration algorithm nominally removes the effects of this unwanted reflection from the measurements, it is still physically present, and it affects the overall sensitivity of such sensors. Accordingly, fully matched designs have been employed by some workers [7], in which the outer and inner diameters are changed in the bead region (respectively expanded and reduced) to retain the same characteristic impedance throughout (typically 50Ω). The steps in the conductor diameters produce discontinuity fringing capacitances which can themselves be compensated for across a broad frequency band by undercutting the bead, i.e. by making it slightly shorter than the section of line that contains it – see Figure 4. The fringing capacitances can be calculated by using a modal analysis [8]. The procedures to be followed here have been well established over many years in the design of matched beaded coaxial connectors, such as PC-7 connectors. They are discussed further in [9][10][11][12].

Figure 3: NPL 15.1 mm, 7 mm, 3.5 mm coaxial sensors and (at the right) the Agilent model HP 85070A. The specified sizes refer to the bore of the outer conductor. Flange diameters are 50, 25, 12 and 19 mm respectively.

Provided that the flange has a sufficiently large diameter, the sensor, to a good approximation, has the so-called *infinite half-space* geometry, which has the advantage of being *analytically calculable*; i.e. computation of reflection coefficient is tractable by using analytical techniques. In general, a flange diameter of about three times the outer conductor internal diameter is sufficient [13]. However, effects attributed to flange resonances [4] [14] occur at higher frequencies when measuring high-permittivity liquids that have $\tan\delta < 0.3$ (approx.). Further discussion of the effect of a finite flange diameter has been given in [15], which also proposes an analytically calculable solution for this case. FDTD methods can also be applied to sensors that have a finite-diameter flange [16].

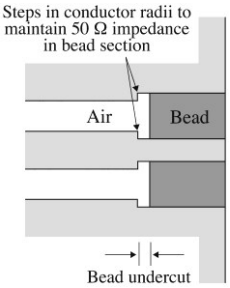

Figure 4: Matched coaxial sensor design. Steps in the conductor radii (needed to maintain line impedance) give rise to fringing capacitance, which is compensated for by undercutting the bead.

For a 15.1-mm sensor with a 50-mm flange immersed in water the lowest resonance occurs at approximately 580 MHz (Figure 5). For a 7-mm sensor with 25-mm diameter flange this resonance occurs at approximately 1.1 GHz and is much weaker. The lowest-frequency resonant mode most likely to be encountered is the TM_{01} mode [14]. At resonance, one half-wavelength of the signal in the medium of the sample is observed to be very approximately the difference between flange and bore diameters. Another important consideration is that the depth of penetration of the fields [17][18] is greater for larger sensors, so for finite volumes of such liquids there will be reflections from boundaries [7]. These may cause volumetric resonances [14]. For ~ 3.5 mm and smaller sensors boundary and flange effects are generally negligible provided that an adequate sample volume is used. This can be explained as follows: (i) for a small sensor the fields have a short range, (ii) small dimensions imply a higher flange resonant frequency and therefore increased damping from dielectric loss in Debye liquids such as water (Debye relaxation frequency ~ 17 GHz at 20 ºC).

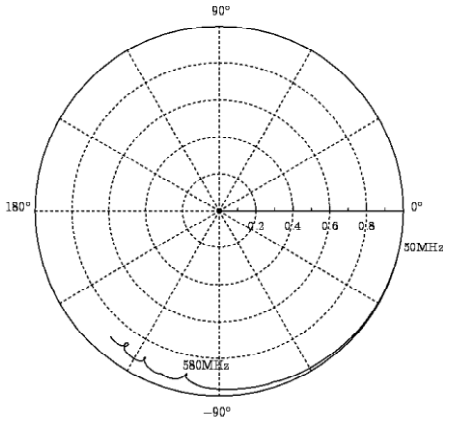

Figure 5. Observed S_{11} trace for water measurement using a 15.1-mm coaxial sensor with 50-mm diameter flange over the frequency range 50 MHz to 1 GHz. Flange resonances can be seen to occur at 580 MHz and higher frequencies.

The outcome of a *full-wave* modal analysis of the coaxial sensor infinite half-space geometry based on Maxwell's equations is an expression for the admittance of the coaxial sensor in the form of an integral, for which there is no analytical solution. In [19][20][21][22][23][24][25] numerical methods of solution are described (see also the review [26]). Until quite recently, desktop computers were not fast enough for rapid on-line computation of results, so various approximate techniques [5][26][27] that are less computationally demanding were devised. The speed of PCs has improved so much that results can now be computed on-line using software based on a full-wave analysis. In this paper results are computed using computer software written by Warham [20]. This software has been validated by intercomparisons [28]. Validation is an essential aspect of traceability in software-dependent measurements. The algorithms actually compute complex reflection coefficient from sample permittivity ε*. To obtain ε* from reflection coefficient measurements the calculation is inverted using an iterative routine. A *gradient descent* method (using numerical first-order differentiation) is easily implemented in software, and gives rapid convergence.

Prior to measurements using a coaxial sensor, a calibration must be performed. This corrects for mismatches and defines a reference plane for measurements located at the face of the sensor, using a bilinear correction formula. By far the most common method for calibration uses a *reference liquid* [29]. This requires measurements with the sensor short-circuited, open-circuited (i.e. radiating into air), and immersed in a reference liquid. From these three measurements, correction coefficients can be found. In order to perform this calculation the actual reflection coefficients of the three measurements must be assumed to be known: these reflection coefficients are referred to here as the 'defined' reflection coefficients. For subsequent measurements to be traceable, the 'defined' reflection coefficients must also be traceable. The short-circuit measurement has a nominal reflection coefficient of –1.0, but can be prone to contact problems (see Section 5), so a least-squares calibration algorithm has been developed to improve the reliability of measurements. This will be discussed in Section 4. The reflection coefficients of the coaxial sensor when immersed in the reference liquid are also calculated by using software. This requires the complex permittivity of the reference liquid to be known at the measurement temperature. Therefore, it is essential to use reference liquids for which accurate and traceable data is published. Comprehensive data on a number of liquids have been published (see Section 3). In the authors' experience this reference liquid calibration method (with open circuit, short-circuit and reference liquid) is the most satisfactory for the majority of the sensors that approximate to the infinite half-space geometry, if carried out with due care. A second reference liquid can be used instead of the short circuit. This may be appropriate if a good short-circuit contact is difficult to obtain, e.g. for very small sensors. The reference liquid method has the advantage that some systematic uncertainties are reduced if the calibration reference liquid and samples being measured have similar dielectric properties [30]. It is also possible to calibrate by using mechanical artefacts, which give more direct traceability to impedance reference standards (which are generally traceable to measurements of dimensions). Some published methods are listed below:

i) Instead of a reference liquid, an open-circuit with increased capacitance can be made using a "short cavity" placed at the measuring face of the sensor [31]. This is a calculable geometry. A limitation for this technique for small sensors is that the capacitance is highly sensitive to the length of the cavity, which must be small to give a high capacitance.

ii) The sensor flange may be replaced by a "substitute connector" to enable calibration using artefact coaxial

Published version at http://dx.doi.org/10.1088/0957-0233/18/5/026

impedance standards [7]. The technique requires that the internal dimensions and the bead of the substitute connector are practically identical to those of the flange.

iii) The body of the sensor may be a fully calculable structure having known dimensions, in which case calibration can be carried out at the end of the test-port return cable (using artefact standards) prior to attaching the sensor. A de-embedding process [32] is used to relate the measured reflection coefficient to that at the face of the flange.

iv) For a sensor that is matched to the test-port (as shown in Figure 4) a two-stage process can be followed, in which a "refresh" or "secondary" calibration is carried out after an initial full calibration at another reference plane [33]. For example, a calibration may be performed at the end of the test-port return cable by using artefact coaxial reflection-coefficient standards. Then with the sensor attached a measurement can be performed (typically with the sensor open-circuited, i.e. radiating into air) to correct for its electrical length and loss. Electronically-switched devices have been developed to enable the calibration process to be automated [33].

3. Dielectric Reference Liquids

In this section the suitability of various reference liquids for calibrating coaxial sensors and as check standards is discussed, and some publications that provide data are cited. Several factors need to be considered when selecting reference liquids. These include the size of the coaxial sensor, the measurement frequency range and the availability of reference data that is traceable to international standards. Uncertainties tend to be smaller if the calibration reference liquid and sample have similar properties, although this is not always possible as the range of suitable well-characterised polar reference liquids is actually quite limited. Measurements made using coaxial sensors that have apertures larger than about 7 mm on comparatively low loss ($\tan\delta < 0.3$) high-permittivity, liquids such as water, may be affected by flange and volumetric resonances (Section 2). Some of the measurements presented in Section 7 illustrate the errors that can occur if poor choices are made. If these effects occur during calibration measurements, subsequent measurements on samples are likely to have large errors.

Table 1 provides information to aid the selection of reference liquids and the size of sensor – choices that cannot be made independently. Note that the largest suitable sensor usually will give the best results. As an example, for measurements on the TEMs that are used in mobile telecommunications SAR measurements (400 MHz to 6 GHz), a 7 mm sensor calibrated by using ethanol as a reference liquid is a usually the best choice. However, a 3.5 mm sensor calibrated using pure water can also give good results. For measurements below ~500 MHz, 15 mm and larger sensors offer the best sensitivity (see Section 7.4). In this frequency range a number of reference liquids are suitable for calibration, e.g. water, methanol and ethanol.

Table 1: Recommendations for suitability (Yes/No) of various liquids and sizes of coaxial sensor for measurement in four frequency bands.

Size	Liquid	30 – 130 MHz	100 – 500 MHz	400 MHz – 6 GHz	6 – 18 GHz
15.1 mm	Aqueous solutions	Y[1]	Y	N	N
	Methanol	Y[1]	Y	N	N
	Ethanol	Y[1]	Y	Y[3]	N
	Telecomms SAR[5]			N	
	MRI SAR[6]	Y[1]			
7 mm	Aqueous solutions	N	Y[1]	Y[2]	N
	Methanol	N	Y[1]	Y	N
	Ethanol	N	Y[1]	Y[3]	N
	Telecomms SAR[5]			Y	
	MRI SAR[6]	N			
3.5 mm	Aqueous solutions		Y[1]	Y	Y
	Methanol		Y[1]	Y	Y[3]
	Ethanol		Y[1]	Y[3]	Y[3,4]
	Telecomms SAR[5]			Y	
	MRI SAR[6]	N			

[1] A larger sensor will give better accuracy at these frequencies.
[2] Flange resonances are small but detectable for pure water, so not ideal. Ionic solutions are lossier, so problems are less likely.
[3] If using as a reference liquid, note that the single-Debye model is not accurate enough for the whole of this frequency range.
[4] Not recommended for calibration as the permittivity is low.
[5] Coaxial sensors are often used to characterise Tissue-Equivalent Materials used in SAR measurements. These are mixtures designed to have similar complex permittivity to human tissues. At telecommunications frequencies (400 MHz – 6 GHz), typically $\varepsilon' \sim 40$-55 and $\tan\delta > 0.4$.
[6] Tissue-Equivalent Materials used in assessing SAR of Magnetic Resonance Imaging (MRI) systems at 30-130 MHz – see Section 7.4.

Sources of data for the most commonly used reference liquids, pure methanol, ethanol and water, are cited below and in two recent publications [5] and [34]. The latter also discusses how to use reference liquids correctly. The electromagnetic behaviour of polar liquids is often described by relaxation models [35] (e.g. Debye, double Debye, Davidson Cole), which are convenient as they enable complex permittivity to be calculated at any frequency. However, such models can only be accurate over a limited frequency range. Reference data is often only available in

5º C steps, as a function of temperature, but values for ε^* at intermediate measurement temperatures can generally be found with sufficient accuracy by using linear interpolation.

Ethanol is often chosen for calibrating sensors larger than ~3.5 mm at RF and microwave frequencies, as it has sufficient loss at the frequencies at which flange resonances and boundary effects might be expected to ensure that they have negligible effect. A single-Debye relaxation model provides an adequate description of its dielectric behaviour up to only ~ 2 GHz. In [36] traceable permittivity data are given at frequencies up to 5 GHz. Data at higher frequencies are given in [37] and [38]. In the microwave range ε' falls with increasing frequency – for ethanol from ~ 25 at 100 MHz to ~ 5 at 5 GHz (at 20 ºC). Nevertheless, for a 7-mm sensor immersed in ethanol, the reflection coefficient is still sufficiently different from that of an open-circuit (air) measurement at 5 GHz to make it an acceptable standard.

Methanol is also useful as a reference liquid. It has a higher static permittivity and higher relaxation frequency than ethanol. However, for large sensors flange and boundary and resonance effects are significant, e.g. at ~ 1 GHz and above for a 15mm sensor. In [36] traceable permittivity data are given at frequencies up to 5 GHz. Data at higher frequencies are given in [39]. For use in coaxial sensor measurements, the single-Debye relaxation model seems to be adequate up to at least 6 GHz.

Pure water is the best characterised of all polar liquids [40][41]. It can be described by a simple single-relaxation Debye model at frequencies of up to at least 30 GHz [42]. Deionised water can usually be considered to have identical properties to pure water for practical purposes. Water is often used as a reference liquid for calibrating ~3.5 mm or smaller sensors as it has the advantages of being low cost, freely available and non-toxic. However, as a consequence of poor wettability, air bubbles often form on the flange. These must be removed manually otherwise measurement errors will occur (see Section 5). For a 7-mm sensor with 25-mm diameter flange, water is not the ideal choice as a calibration reference liquid because resonance and boundary effects are visible at frequencies above ~1 GHz. For larger sensors problems occur at lower frequencies and are more severe.

Acetone is one of the few pure liquids that has high-permittivity at millimetre-wave frequencies besides water. As is the case for water, at low microwave frequencies it has comparatively low loss, so flange and volumetric resonances may occur with larger sensors. Note that some polymers are affected by acetone. Static permittivity data for acetone is available in [36]. Relaxation parameters for acetone at 20 ºC have been published [43]. There is little other published data on acetone at the present time.

Solutions of ionic salts of known concentration can in principle also be used as calibration standards. These have greater loss than pure water, particularly at frequencies below 1 GHz, so flange resonance and boundary effects should be reduced in magnitude at these frequencies. Data for NaCl and KCl solutions are available in a number of publications, e.g. [44] [45] [46] [47]. Much of the data available in the literature has been derived by using time domain methods, or by using coaxial sensors calibrated with other reference liquids. There is little published work on uncertainties and traceability of dielectric measurements by these methods. Users should be aware that salt solutions may cause corrosion of metal artefacts. Changes to the apparent dielectric properties are caused by electrode polarisation effects [34] [48]. These effects depend on concentration, but reduce with increasing frequency. For pure water they are generally negligible at frequencies above ~ 200 kHz [49], but for ionic solutions they can extend into the 10–100 MHz range. Ionic solutions can be prepared from weighed anhydrous salt crystals.

4. An Algorithm for Least Squares Calibration

In this section a least-squares calibration algorithm for calibration of reflectometers such as one port of a Vector Network Analyser (VNA) is described. The least-squares approach to calibration enables confidence in calibrations to be increased, and uncertainties reduced. If least-squares calibration is used, poorly-contacting short-circuit measurements (a common problem with coaxial sensors) can be identified from residual calibration errors.

The calibration of reflectometers is based on a bilinear transform which defines a phase reference plane and a magnitude scale, and corrects for mismatches:

$$Z = \frac{aW + b}{cW + 1} \qquad (1)$$

In the above equation, the *'defined' and 'indicated'* complex reflection coefficients are represented by Z and W respectively. The complex coefficients a, b and c are determined by a calibration process [50][51][52]. Three sets of calibration data, (Z_1, W_1), (Z_2, W_2), and (Z_3, W_3) are sufficient to determine the complex coefficients a, b and c uniquely at each frequency. For reference liquid and open-circuit measurements, the defined complex reflection coefficients are calculated at each frequency by using software. The defined complex reflection coefficient of a short-circuit is $Z = -1+j0$ at all frequencies (assuming perfect contact and assuming inductance to be negligible). For a measurement system which is affected by uncertainties, such as short-circuit non-repeatability in the case of a coaxial sensor, then it is often beneficial to use more than three calibration measurements, in which case a, b and c will be over-determined. Optimum values can then be found by using a least-squares process. A simple algorithm to achieve this is described below:

For the ith calibration measurement we may write:

Published version at http://dx.doi.org/10.1088/0957-0233/18/5/026

$$Z_i \to Z_i + \Delta Z_i \qquad \text{and} \qquad W_i \to W_i + \Delta W_i$$

where ΔZ_i and ΔW_i represent errors in the definition and measurement. It is possible to substitute the above in (1), and perform a generalised distance regression [53] to minimise all ΔZ_i and ΔW_i at once. The simpler but approximate strategy used here is to minimise ΔW_i only. Making the substitution $W_i \to W_i + \Delta W_i$ in equation (1) gives:

$$\Delta W_i = \frac{cZ_iW_i + Z_i - b - aW_i}{a - cZ_i} \qquad (2)$$

The optimum values of *a*, *b* and *c* satisfy simultaneously the three conditions

$$\frac{\partial}{\partial q}\sum_{i=1}^{i=N} \Delta W_i P_i \Delta W_i^* = 0 \qquad (3)$$

in which *q* represents *a*, *b* and *c* in turn, *N* is the total number of measurements and *P* is an optional weighting factor for each measurement. The result of the optimisation will not depend that critically on the values of *a* and *c* in the denominator, so as an intermediate step a reasonable approximation can be made by replacing them with constant values a_0 and c_0. Assigning

$$Y_i = \frac{1}{a_0 - c_0 Z_i} \qquad (4)$$

and substituting in eqn. (2), we obtain the linear equation

$$\Delta W_i = cZ_iW_iY_i + Z_iY_i - bY_i - aW_iY_i \qquad (5)$$

The Y_i values may all be set to 1.0 to enable an approximate (but reasonably accurate) solution for *a*, *b* and *c* to be found by using the method of linear least squares. To obtain an improved solution, these may be used as initial values for a method such as Gauss-Newton. Alternatively, when $|c| << |a|$ (which for this type of measurement is generally the case), it is sufficient to repeat the least-squares process outlined above in a loop until the solution is no longer changing significantly. At the beginning of each loop the assignments $a_0 = a$ and $c_0 = c$ are made, and all Y_i are re-calculated.

Optimum values of *a*, *b* and *c* (in equation 2) can also be found by using a least-squares minimisation function from a software library, such as NAG [54] function E04FCF. It is found that E04FCF allows convergence to a solution even when initial estimated values are very approximate.

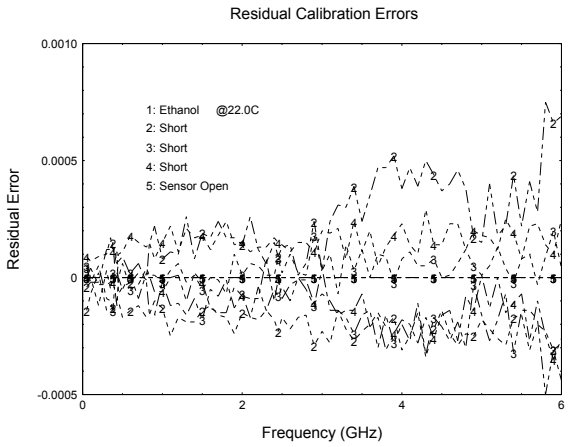

Figure 6: Residual calibration errors of a least-squares calibration as a function of frequency. The real and imaginary parts of the residual reflection-coefficients of the calibration artefacts are shown on the y axis. The measuring instrument was an Agilent model 8753ES VNA (settings: *Averaging Factor* 4, *IF bandwidth* 100 Hz).

Figure 6 shows a typical set of residual errors arising from a calibration using a reference liquid, open-circuit and three short-circuits. The residual errors are given by

$$R_i = Z_i - \frac{aW_i + b}{cW_i + 1} \qquad (6)$$

for each calibration measurement. By inspection of such plots, inconsistent short-circuit measurements can be identified. The technique can be used for any combination of calibration artefacts provided that at least three of them have different reflection coefficients, so for example, additional reference liquids can also be included in the calibration.

5. Calibration And Measurement Procedure

The coaxial sensor is connected to the VNA by means of a high quality, phase stable, test-port return cable. To minimise disturbance to the cable, the sensor is held in a clamp. Phase stability is also affected by temperature variations, so a temperature-controlled laboratory is required for the best results. The flange is immersed in (and completely covered by) the liquid. To assist in the removal of air bubbles when measuring liquids, the coaxial sensor can be positioned so that its flange is at a slight angle from horizontal.

Figure 7: Clamp for foil short-circuit

Obtaining an accurate and traceable VNA calibration is particularly important, as it affects all subsequent measurements. The method preferred by the authors and described here uses three short-circuit measurements, an open-circuit measurement, and a measurement on a reference liquid. Guidance on selecting reference liquids is given in Section 3. In-house software that uses the algorithm described in Section 4 is used for least-squares calibration. During the open-circuit measurement the face of the sensor must be clean and dry. Short-circuits are obtained by using a small piece of clean copper foil (approx. 15 x 15 x 0.05 mm). For 7 mm and smaller coaxial sensors, much improved contact repeatability is obtained if the foil is pressed firmly against the sensor with the aid of a rubber cone with rounded tip in a clamp (Figure 7). It is found that the best contact is obtained when the foil is rotated against the sensor by a quarter of a turn when under pressure. To ensure that any inconsistency in the contact is represented in the residual errors, the foil contact is broken then re-made between the three measurements. Following the calibration, the residual errors are plotted (see Figure 6). If the residual errors are larger than expected then the short-circuit measurements are repeated. Whichever method of calibration is used, it is recommended that a 'check' measurement is performed upon a reference liquid. This should have significantly different dielectric properties from those of the calibration reference liquid, if used.

Certain aspects of experimental technique need to be considered carefully if accurate measurements are required:

Minimise boundary and flange effects: As noted in Section 2, flange and volumetric resonances occur with 7-mm and larger coaxial sensors when measuring high-permittivity liquids that have $\tan\delta < 0.3$ (approx.). The proximity of a boundary has an effect on the flange resonance, so the effects are inter-related. Evidence for such effects can be found experimentally, e.g. in measurements on aqueous samples contained in a 65-mm diameter by 40-mm deep vessel when using a 7-mm coaxial sensor with 25-mm diameter flange. In this case a ~1 cm displacement of the vessel may change the measured reflection coefficient trace displayed on the VNA significantly at frequencies above ~1 GHz. If the sensor is placed more-or-less centrally in a larger vessel, e.g. 90-mm in diameter by 50-mm in depth, these effects are much reduced (measurements are presented in Table 6). It is particularly important that calibration measurements on reference liquids are free from these effects. For this reason there is considerable merit in choosing a high loss liquid (see Section 3) for calibration.

Measure the temperature of reference liquids: The complex permittivity of polar liquids often has a high temperature coefficient. Therefore, it is recommended that the temperature of liquid samples should be recorded to the nearest 0.1 ºC. During the computation of calibration coefficients, the Z_i reflection coefficients for the calibration reference liquid must be calculated from the complex permittivity at the actual measurement temperature.

Remove air bubbles: To obtain reliable measurements it is important that air bubbles at the face of the sensor should be removed before liquids are measured. Bubbles are not usually a problem for alcohols as they have low surface tension, but they often cause difficulties when measuring water and aqueous solutions, as well as more obviously viscous materials. A spatula can be used to drive away visible bubbles. It has been found that bubbles too small to be visible easily to the naked eye (i.e. smaller than ~ 0.2 mm) can be present, and can reduce the measured ε' for an aqueous sample by as much as 1%. A malleable implement is more effective than a hard one for removing these.

Take precautions to avoid contamination of liquids: When using hygroscopic liquids, such as methanol and ethanol, it is essential that fresh samples from sealed bottles are used.

6. Estimation Of Uncertainties By Monte-Carlo Modelling

Uncertainties of coaxial sensor measurements vary considerably according to the measurement frequency and the complex permittivity of the sample being measured. Reference liquids having similar properties to sample dielectrics (but *not* the calibration reference liquid if one is used), can be used for making estimates of uncertainty, but this procedure is rather *ad hoc*, and often not possible due to lack of suitable liquids.

A more generally applicable approach is to use Monte-Carlo Modelling (MCM) [55][56][57][58], which allows estimated input uncertainty distributions to be propagated through a complex model that is implemented in software, to yield corresponding output distributions. It requires a series of "trials" to be set up, in which simulated input parameters such as dimensions and measurements data are varied randomly in accordance with a selected statistical distribution, such as the normal distribution. Given a sufficient number of trials, the corresponding distribution of the complex permittivity and its standard uncertainty can be found. The uncertainties obtained actually apply to a randomised population of coaxial sensors. The MCM approach described here was first introduced by the authors in [59], but has since been improved.

The calibration and use of a coaxial sensor requires a number of stages (the entire process is represented schematically in Figure 8). The MCM is complete in the sense that it takes all of these into account, including calibration. Hence there are contributions relating to the VNA and cable, calibration liquid, reference data,

temperature, and the sensor itself, e.g. dimensions. The input parameters appear at the left-hand side of Figure 8. At the beginning of each trial, values for the inputs are obtained by using a pseudo-random number generator. Normal distributions centred on the nominal value are assumed. An important consequence of using a comprehensive model is that many of the input parameters are independent and can be taken to be uncorrelated. The modal analysis that is used for calculating the reflection coefficient of the sensor from dimensions and complex permittivity uses a finite number of modes, and therefore has an associated numerical uncertainty. The modal-analysis module is used three times in the process shown in Figure 8, each of which is given an independent numerical uncertainty contribution in each trial.

The simulation is slow to run so it was necessary to restrict the number of trials. In general, the more input parameters there are in an MCM, the more trials are needed to produce stable outputs. However, when a few of the contributions are dominant, as is the case here, the minimum number of trials needed is reduced. It is found that ~200 trials are required to produce acceptably stable output. The simulated uncertainties presented in this paper were calculated from 1000 trials. Using a modern PC, the simulation takes a few minutes per frequency.

Confidence limits can be estimated from the outputs (as a sorted list) directly, no matter what shape a distribution has. For distributions that are approximately normal, the standard uncertainty can be taken to be the standard deviation of the distribution to a reasonable approximation, and this approach has been adopted here.

One of the aims of this paper is to demonstrate that uncertainties estimated by MCM are consistent with measurements over a range of frequencies for several samples that have a range of complex permittivities. Every effort has gone into making the model as comprehensive as resources allowed, but the following limitations are recognised:

The bead may absorb liquids to some extent, which may change its permittivity. The NPL sensors referred to in this paper use beads made from the polymer Rexolite, which according to its manufacturer has low absorption (less than 0.05% by weight). The effect of small changes occurring during the measurement process is simulated in Table 2. A uniform bulk change in ε' is assumed.

Boundary and flange effects (discussed in Sections 2, 3 and 5) are not accounted for in the Monte-Carlo process, but can be estimated experimentally and treated as an additional uncertainty contribution.

The effects of hygroscopicity of the ethanol calibration liquid and measured samples is not specifically accounted for. In the measurements presented in this paper, fresh samples of liquids were used, and the measurements were made in a minimum amount of time.

Geometrical imperfections such as non-planarity between bead and conductors at the face of the sensor are not accounted for. As stated in Section 3, when the sample and the calibration reference liquid have similar complex permittivity some uncertainties contributions are reduced, geometrical imperfections are among these. It is possible to model geometrical imperfections by using techniques such as FDTD [16][60]. Explicit expressions for the effect of imperfections on reflection coefficient, even if only approximate, can in principle readily be incorporated into the Monte-Carlo Modelling of uncertainties. However, no such expressions have been published to the knowledge of the authors.

Effects due to Temperature will occur if the sensor is calibrated and used respectively at two different temperatures. Approximate corrections for expansion can be made, but experimental evidence presented in Section 7.2 (based on reference liquid measurements) shows that these are unnecessary in the range 20 – 40 ºC for the stable precisely-machined designs of sensor described in this paper. Simple probes made from truncated semi-rigid cable are less stable mechanically, and are reported to be very sensitive to the effects of temperature [61]. The permittivity of the bead will vary with temperature T, but the variation is small (for common polymers $\Delta\varepsilon'/\Delta T \sim -5\text{x}10^{-4}$ per °C, see [62]). In [63] and [64] the application of coaxial sensors over a much larger range of temperature is discussed.

MCM was used to estimate contributions as shown in Table 2 at 0.1 GHz and 2.45 GHz for measurements on methanol. Note that standard uncertainties are quoted [65]. At the lowest frequencies the sensor becomes less sensitive (see Figure 2), which is consistent with the observation that at 0.1 GHz the numerical accuracy of the software and the VNA detector noise are the dominant contributions. If needed, the accuracy of the software can be improved, e.g. by increasing the number of modes. At 2.45 GHz the importance of choosing a good quality test-port return cable and subjecting it to minimal twisting and bending (e.g. by using a clamp) is evident. A linear dependence of phase uncertainties on frequency is assumed, so this uncertainty contribution increases with frequency. In order to obtain accurate estimates of uncertainty it is advisable to assess the actual cable that is to be used, as cables can vary considerably. It should also be noted that they deteriorate in use and need to be checked periodically.

Table 3 gives the overall uncertainties presented at coverage factor 2 (approx. 95% Confidence Level) obtained by MCM using all of the contributions listed in Table 2.

Table 2: Monte-Carlo Modelling of uncertainties of measurements on methanol at 22°C made with the NPL 7-mm coaxial sensor calibrated by using a reference liquid (ethanol). The uncertainty contributions shown are all standard uncertainties.

Monte-Carlo input data				Contrib. at 0.1 GHz		Contrib. at 2.45 GHz	
Name	**Nom. Value**	**Standard unc.**	**Distribution**	$\sigma_{MCM}(\varepsilon')$ [g]	$\sigma_{MCM}(\varepsilon'')$ [g]	$\sigma_{MCM}(\varepsilon')$ [g]	$\sigma_{MCM}(\varepsilon'')$ [g]
Bead permittivity	2.54 [a]	± 0.01	Normal distributions are assumed	< ± 0.001	< ± 0.001	± 0.0025	± 0.0006
Change in bead permittivity [k]	0	0.002		± 0.013	< ± 0.001	± 0.008	± 0.005
Outer radius (mm)	3.348	± 0.005 [b]		< ± 0.001	< ± 0.001	± 0.0015	± 0.0015
Inner radius (mm)	1.002	± 0.005 [b]		± 0.001	< ± 0.001	± 0.0049	± 0.0041
VNA detector noise	0	± 0.0002 [c]		± 0.13	± 0.13	± 0.019	± 0.021
Numerical error in calculation of refl. Coefficient	0	± 0.0003 [c]		± 0.12	± 0.18	± 0.013	± 0.022
Phase-1 [i] (° per GHz)	0	± 0.05 [d]		± 0.034	± 0.001	± 0.050	± 0.018
Phase-2 [j] (° per GHz)	0	± 0.02 [d]		± 0.02	± 0.002	± 0.05	± 0.014
Ref. Liquid Data [e] ε_s	25.16	± 0.02		± 0.028	± 0.001	± 0.011	± 0.015
Ref. Liquid Data [e] ε_H	4.486	± 0.013		< ± 0.001	± 0.002	± 0.026	± 0.019
Ref. Liquid Data [e] f_r (GHz)	0.834	± 0.002		± 0.001	± 0.008	± 0.036	± 0.025
Ref. Liquid Data [e] Γ	0.051	± 0.003		< ± 0.001	< ± 0.001	± 0.006	± 0.020
Temperature non-uniformity of reference liquid (°)	0	± 0.1 [h]		± 0.024	± 0.013	± 0.032	± 0.017
Thermometer reading (°)	22.0	± 0.13 [l]		± 0.018	± 0.01	± 0.043	± 0.023
Short-circuit contact	-1+j0	± 0.0002 [c]	Modified normal [f]	< ± 0.001	< ± 0.001	± 0.0005	< ± 0.0001

[a] Lucentine (equivalent to rexolite) material measured by using a split-post dielectric resonator.
[b] The measured uncertainty is ± 0.001 mm, but an increased value is used to account for corner radii.
[c] Uncorrelated equal contributions to both real and imaginary channels are assumed. The figure applies to Agilent model 8753ES VNA, set to: *IF Bandwidth* 100 Hz, *Averaging* 4.
[d] For a phase-stable cable subjected to minimal movement.
[e] Debye data for ethanol from [36]. Values at 20 °C are shown. The quantity Γ describes the effect of the second Debye relaxation (a low-frequency approximation is used).
[f] The reflection coefficient of a short-circuit approaches but can never exceed unity. So trials that have magnitude greater than unity are discarded.
[g] Standard deviation of the output distribution of ε' or ε'' determined by Monte-Carlo Modelling. Quoted as standard uncertainty, i.e. without multiplication by a coverage factor.
[h] Due to evaporative cooling.
[i] Phase-1 refers to phase drift. It is estimated from open-circuit measurements (i.e measurements on air) after a period of use in a temperature-controlled laboratory. A high-quality VNA test-port return cable is used.
[j] Phase-2 is a separate phase contribution that is applied to the calibration measurements. Since the calibration process only takes a few minutes, and the cable is subjected to minimal disturbance, this is smaller than Phase-1. The phase errors for each calibration measurement are assumed to be independent.
[k] The permittivity of the bead may be increased due to absorption of liquids. This contribution simulates a hypothetical change in bead permittivity that occurs between calibration and the measurement on the sample. It is estimated from measurements on a disc sample before and after immersion in methanol by using a split-post dielectric resonator.
[l] The uncertainty in the measurement temperatures of the Debye data for ethanol from [36] and the uncertainty of the temperature measurement during calibration of the coaxial sensor combined.

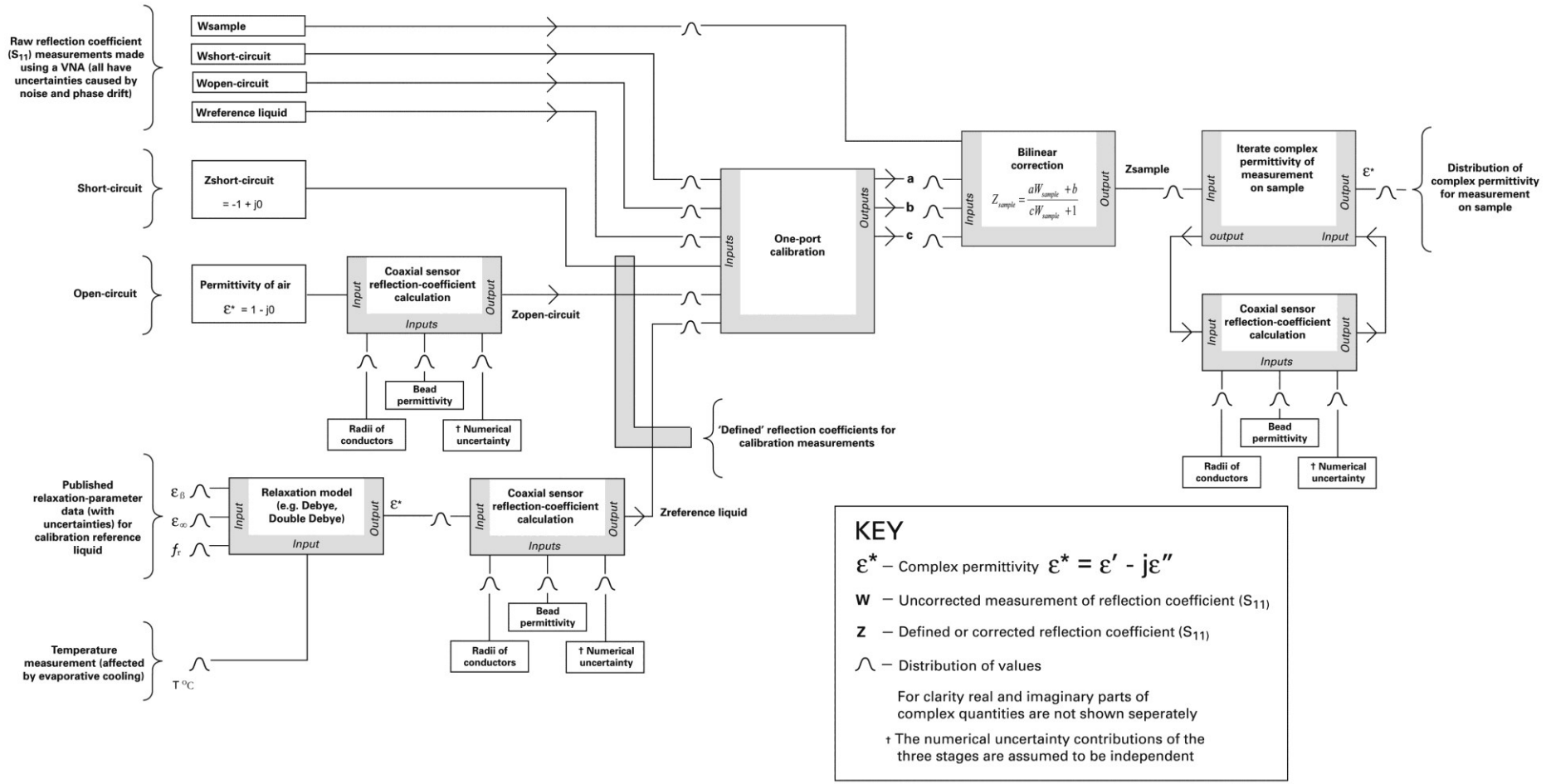

Figure 8: Schematic of Monte Carlo process for estimating uncertainties of coaxial sensor measurements

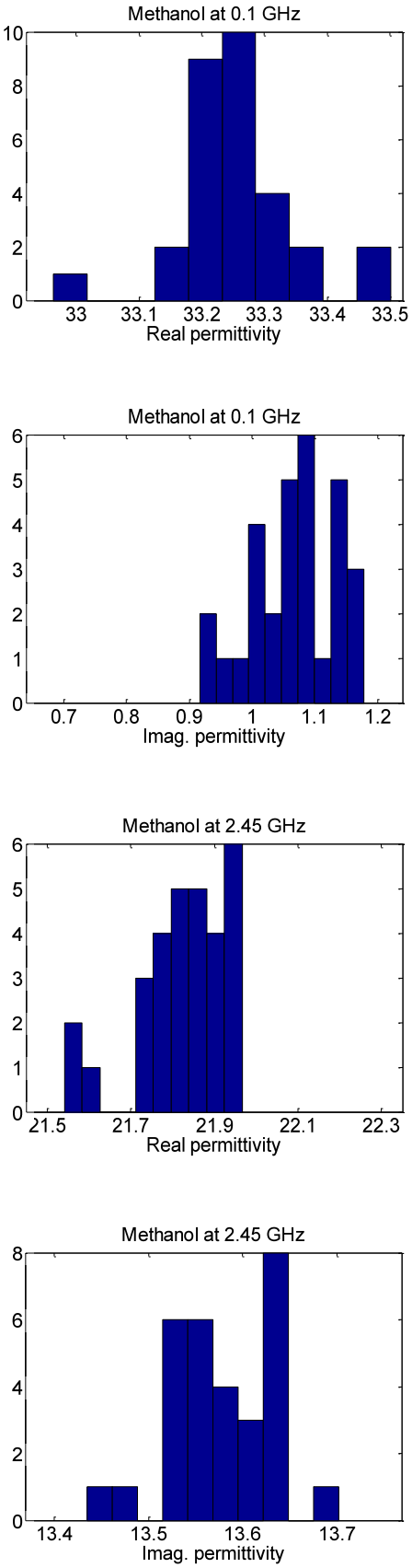

Figure 9: Histograms of methanol measurements (from 30 separate experiments carried out over a period of a year). All data is shown corrected to 22 ˚C.

Table 3: Estimated uncertainties of measurements on methanol at 22 °C using the NPL 7-mm coaxial sensor. They are estimated by a Monte Carlo Modelling and are presented at coverage factor *k=2*, i.e. approx. 95% Confidence Level.

Freq. GHz	**ε´ Unc.**	**ε´´ Unc.**
0.1	± 0.37	± 0.44
2.45	± 0.22	± 0.13

Table 4: Reference data for methanol at 22°C [36]. Uncertainties are presented at coverage factor *k=2*, i.e. approx. 95% Confidence Level.

Freq. GHz	**ε´**	**Unc.**	**ε´´**	**Unc.**
0.1	33.22	± 0.06	0.94	± 0.01
2.45	21.90	± 0.16	13.57	± 0.10

7. EXPERIMENTAL INVESTIGATIONS

7.1 Comparison of MCM Predicted Uncertainties With Repeatability of Measurements On Methanol

Figure 9 shows histograms of measurement results on methanol at 0.1 GHz and 2.45 GHz that were made using a 7-mm coaxial sensor with a 25-mm diameter flange. In each case, calibration was by the reference liquid method, using ethanol as the reference liquid. The data presented are the methanol check liquid measurements obtained in a series of experiments performed over a period of one year. These measurements were each deemed by the operator to show satisfactory operation of the sensor. The body of liquid in each case was approximately 70 mm in diameter by 40 mm deep. Experimentally this was found to be sufficient to avoid significant flange or volumetric resonances at these frequencies. In each experiment the residual calibration errors were plotted and checked, as shown in Figure 6. They were typically of the order ± 0.0005, which shows that for each calibration the three short-circuit calibration measurements were consistent.

Despite the small sample size, the distributions of the methanol measurements in Figure 9 perhaps suggest a Gaussian (normal) shape, although some asymmetry is evident. Simulations have shown that the asymmetry of the distributions that is observed is not a consequence of lack of numerical precision in the modal analysis [20] or the iterative processes used in the software used for processing the data. The measurement temperatures of the methanol samples varied, but were almost all in the range 21-22 ºC. The data shown is corrected to 22 ºC. The x-axes of the graphs are centred on the expected values shown in Table 4. Since the samples were measured in open beakers, temperature measurement accuracy is affected by evaporative cooling, but this is not large enough to be a dominant factor – the change in complex permittivity ($\varepsilon^* = \varepsilon' - j\varepsilon''$) is -0.02 - j0.003 per 0.1 ºC cooling at 0.1 GHz, and is 0.016 - j0.014 per 0.1 ºC cooling at 2.45 GHz.

The histograms shown in Figure 9 may be compared to the uncertainties estimated by MCM given in Table 3. There is good agreement between the spread of the experimental data and the predicted uncertainties (which are given at 95% Confidence Level), despite the fact that the histograms show only the effects of random errors. Comparison may be made to the reference data for methanol in Table 4. This shows that MCM can provide valid estimates of uncertainty for uniform samples when measurements are free from effects such as poor wettability, and flange and volumetric resonances.

7.2 Dependence on Sample Temperature

To show the effect of sample temperature on measurements, methanol and water were measured at temperatures up to 40 ºC with the NPL 7-mm coaxial sensor. For both sets of data, calibration was performed at room temperature using ethanol as the reference liquid. Results are shown in Tables 5 and 6. The final measurement in each table was made after the sample (and sensor) had cooled to room temperature to give an indication of the stability of the system.

No evidence of significant measurement errors caused by the temperature changes can be seen for either sample. The calculated changes in the phase of reflection coefficient due to thermal expansion of the metal body of the sensor are smaller than the Phase-1 uncertainty given in Table 2. The water measurements are to some extent affected by boundary effects caused by the finite size of flange and sample (which are not accounted for in the uncertainty estimates shown), despite the use of a fairly large sample volume (90-mm diameter by 50-mm deep).

7.3 Measurement Intercomparison Using Coaxial Sensors of Different Sizes

Measurements on methanol and dimethyl sulphoxide (DMSO) were made with NPL 15.1 mm and 7 mm coaxial sensors, and the Agilent model HP 85070A – see Tables 7-9 and Figure 3. DMSO is of interest as a reference material as it has similar permittivity to, though is less lossy than, TEMs used for mobile phone SAR measurements. Unfortunately it is very hygroscopic, and when measured in an open beaker temperature *rises* due to absorption of water from the air can be observed. Water absorption inevitably changes the complex permittivity. In these measurements, fresh samples were used to try to minimise this effect.

The nominal size of the Agilent HP 85070A probe is 3.5 mm – larger than the later HP 85070B model [27]. A fine-pitch thread around the bead to provide hermetic sealing and the working face of the flange is not a flat disc as it has an annular recess cut into it. In the measurements presented there is no indication of significant errors caused by these departures from the infinite-half space calculable geometry. NPL in-house software (Warham [20]) was used for processing all of the measurements. To account for the threads the dimensional uncertainties of the conductor diameters are increased in our MCM analysis.

Table 5: Measurements on methanol with the NPL 7-mm coaxial sensor and MCM simulated uncertainties ('Unc' in the table) at a range of temperatures following calibration at room temperature using ethanol as the reference liquid. No corrections for temperature effects such as metal expansion of the sensor were applied. Reference values 'Ref' are taken from [36]. The uncertainties in the 'Ref Unc' columns include the temperature measurement contribution given in column 1. The dimensions of the body of liquid were 65 dia. × 40 mm. For notes to this table, see the key that follows Table 9.

Methanol temperature	**Freq. GHz**	**ε´**					**ε´´**				
		Meas.	**Unc.[p]**	**Ref.[q]**	**Ref Unc.[r]**	**Agree[s]**	**Meas.**	**Unc.[p]**	**Ref.[q]**	**Ref Unc.[r]**	**Agree[s]**
21.7 ± 0.2 ºC	0.45	32.62	± 0.16	32.66	± 0.07	Y	4.24	± 0.17	4.17	± 0.06	Y
	1.0	30.39	± 0.21	30.38	± 0.08	Y	8.47	± 0.13	8.49	± 0.09	Y
	2.45	21.88	± 0.21	21.85	± 0.17	Y	13.58	± 0.13	13.61	± 0.11	Y
	5.0	12.88	± 0.17	12.68	± 0.18	Y	11.91	± 0.15	12.03	± 0.11	Y
29.5 ± 0.2 ºC	0.45	31.38	± 0.15	31.35	± 0.07	Y	3.48	± 0.17	3.38	± 0.06	Y
	1.0	29.79	± 0.21	29.74	± 0.08	Y	7.10	± 0.13	7.04	± 0.12	Y
	2.45	22.96	± 0.21	22.95	± 0.19	Y	12.47	± 0.12	12.42	± 0.14	Y
	5.0	14.10	± 0.18	13.95	± 0.24	Y	12.10	± 0.15	12.30	± 0.14	Y
40.0 ± 0.5 ºC	0.45	29.78	± 0.14	29.58	± 0.11	N	2.74	± 0.16	2.56	± 0.06	N
	1.0	28.80	± 0.18	28.58	± 0.10	N	5.66	± 0.12	5.45	± 0.13	N
	2.45	23.74	± 0.22	23.78	± 0.18	Y	10.90	± 0.12	10.60	± 0.19	N
	5.0	15.63	± 0.19	15.66	± 0.29	Y	12.01	± 0.17	12.15	± 0.17	Y
21.7 ± 0.2 ºC Made after other meas-urements.	0.45	32.83	± 0.15	32.66	± 0.07	Y	4.30	± 0.17	4.17	± 0.06	Y
	1.0	30.55	± 0.20	30.38	± 0.08	Y	8.59	± 0.12	8.49	± 0.09	Y
	2.45	21.90	± 0.21	21.85	± 0.17	Y	13.69	± 0.13	13.61	± 0.11	Y
	5.0	12.84	± 0.17	12.68	± 0.18	Y	11.92	± 0.15	12.03	± 0.11	Y

Table 6: Measurements with the NPL 7-mm coaxial sensor on water and MCM simulated uncertainties ('Unc' in the table) at a range of temperatures following calibration at room temperature using ethanol as the reference liquid. No corrections for metal expansion of the sensor were applied. The reference data 'Ref' is from [40], Table III. The confidence level of the uncertainties given in [40] is not reported, although the data is known to be in good agreement with other publications. The uncertainties in the 'Ref Unc' columns include the temperature measurement contribution shown in Column 1. The dimensions of the body of water were 90 dia. × 50 mm. The tabulated uncertainties are based on the MCM only and do not include allowances for the finite size of flange and vessel, nor poor wettability. For notes to this table, see the key that follows Table 9.

Water temperature	**Freq. GHz**	**ε´**					**ε´´**				
		Meas.	**Unc.[p]**	**Ref. [40]**	**Ref Unc.**	**Agree[s]**	**Meas.**	**Unc.[p]**	**Ref. [40]**	**Ref Unc.**	**Agree[s]**
22.1 ± 0.2 ºC	0.45	78.90	± 0.33	79.39	± 0.16	N	2.13	± 0.40	1.86	± 0.01	Y
	1.0	79.14	± 0.45	79.20	± 0.16	Y	4.06	± 0.35	4.13	± 0.03	Y
	2.45	77.15	± 0.74	78.06	± 0.15	N	9.40	± 0.36	9.96	± 0.07	N
	5.0	72.27	± 1.51	74.05	± 0.14	N	17.45	± 0.96	19.19	± 0.13	N
30.0 ± 0.2 ºC	0.45	76.33	± 0.32	76.53	± 0.21	Y	1.61	± 0.40	1.47	± 0.02	Y
	1.0	76.52	± 0.43	76.41	± 0.21	Y	3.26	± 0.36	3.26	± 0.03	Y
	2.45	75.23	± 0.69	75.67	± 0.21	Y	7.47	± 0.35	7.90	± 0.08	N
	5.0	71.54	± 1.46	73.01	± 0.20	Y	14.11	± 0.80	15.51	± 0.15	N
40.0 ± 0.5 ºC	0.45	72.96	± 0.29	73.16	± 0.21	Y	1.50	± 0.36	1.14	± 0.01	N
	1.0	72.76	± 0.41	73.09	± 0.21	Y	2.65	± 0.34	2.53	± 0.03	Y
	2.45	71.78	± 0.66	72.63	± 0.21	Y	5.75	± 0.32	6.16	± 0.07	N
	5.0	69.88	± 1.45	70.94	± 0.20	Y	11.55	± 0.71	12.26	± 0.13	N
22.1 ± 0.2 ºC Made after other meas-urements.	0.45	78.91	± 0.30	79.39	± 0.16	N	2.24	± 0.40	1.86	± 0.01	Y
	1.0	78.97	± 0.39	79.20	± 0.16	Y	4.05	± 0.35	4.13	± 0.03	Y
	2.45	77.10	± 0.67	78.06	± 0.15	N	9.59	± 0.36	9.96	± 0.07	Y
	5.0	72.14	± 1.45	74.05	± 0.14	N	17.17	± 0.96	19.19	± 0.13	N

Table 7: Measurements and simulated uncertainties made with the NPL 15.1-mm coaxial sensor (flange diameter 50-mm). For notes to this table, see the key that follows Table 9.

Liquid	Freq. GHz	ε′					ε′′				
		Meas.	Unc.[p]	Ref.[q]	Ref Unc.[r]	Agree[s]	Meas.	Unc.[p]	Ref.[q]	Ref Unc.[r]	Agree[s]
Methanol 21.0 ºC ± 0.2 ºC	0.45	32.80	± 0.10	32.78	± 0.13	Y	4.26	± 0.14	4.25	± 0.05	Y
	1.0	30.23	± 0.18	30.43	± 0.08	Y	8.95	± 0.10	8.63	± 0.10	N
	2.45	21.81	± 0.17	21.74	± 0.16	Y	13.53	± 0.14	13.71	± 0.10	N
	5.0	12.81	± 0.12	12.56	± 0.25	Y	11.79	± 0.25	12.00	± 0.10	Y
Dimethyl sulphoxide 22.4 ± 0.2 ºC	0.45	47.00	± 0.19	46.69	± 0.07	N	2.31	± 0.19	2.28	± 0.08	Y
	1.0	46.37	± 0.25	46.18	± 0.07	Y	4.70	± 0.18	5.00	± 0.17	N
	2.45	43.02	± 0.40	43.27	± 0.19	Y	11.03	± 0.19	11.35	± 0.37	Y
	5.0	35.52	± 0.68	35.30	± 0.51	Y	16.61	± 1.23	18.06	± 0.48	N

Table 8: Measurements and simulated uncertainties made with the NPL 7-mm coaxial sensor (flange diameter 25-mm). For notes to this table, see the key that follows Table 9.

Liquid	Freq. GHz	ε′					ε′′				
		Meas.	Unc.[p]	Ref.[q]	Ref Unc.[r]	Agree[s]	Meas.	Unc.[p]	Ref.[q]	Ref Unc.[r]	Agree[s]
Methanol 21.8 ± 0.2 ºC	0.45	32.68	± 0.16	32.64	± 0.07	Y	4.23	± 0.16	4.16	± 0.06	Y
	1.0	30.38	± 0.18	30.38	± 0.08	Y	8.42	± 0.12	8.47	± 0.10	Y
	2.45	22.00	± 0.20	21.87	± 0.16	Y	13.49	± 0.12	13.60	± 0.11	Y
	5.0	13.02	± 0.14	12.69	± 0.18	Y	11.99	± 0.14	12.04	± 0.11	Y
Dimethyl sulphoxide 22.9 ± 0.2 ºC	0.45	47.06	± 0.22	46.63	± 0.07	N	2.47	± 0.24	2.25	± 0.08	Y
	1.0	44.98	± 0.27	46.13	± 0.07	N	4.93	± 0.21	4.95	± 0.18	Y
	2.45	43.16	± 0.39	43.27	± 0.20	Y	11.13	± 0.18	11.25	± 0.38	Y
	5.0	35.88	± 0.42	35.40	± 0.52	Y	17.40	± 0.47	17.97	± 0.50	Y

Table 9: Measurements and simulated uncertainties made with an Agilent HP 85070A coaxial probe (nominal size 3.5 mm, flange diameter 19 mm). VNA calibration and calculation of complex permittivity were performed by using NPL software.

Liquid	Freq. GHz	ε′					ε′′				
		Meas.	Unc.[p]	Ref.[q]	Ref Unc.[r]	Agree[s]	Meas.	Unc.[p]	Ref.[q]	Ref Unc.[r]	Agree[s]
Methanol 22.2 ± 0.2 ºC	0.45	32.71	± 0.29	32.58	± 0.07	Y	4.11	± 0.30	4.12	± 0.06	Y
	1.0	30.58	± 0.26	30.35	± 0.08	Y	8.41	± 0.18	8.39	± 0.10	Y
	2.45	22.10	± 0.26	21.93	± 0.17	Y	13.74	± 0.15	13.54	± 0.11	N
	5.0	12.83	± 0.21	12.76	± 0.19	Y	12.18	± 0.13	12.06	± 0.11	Y
Dimethyl sulphoxide 22.4 ± 0.2 ºC	0.45	47.04	± 0.35	46.69	± 0.07	Y	2.25	± 0.40	2.28	± 0.08	Y
	1.0	46.82	± 0.33	46.18	± 0.07	N	4.96	± 0.27	5.00	± 0.17	Y
	2.45	43.92	± 0.42	43.27	± 0.19	N	11.84	± 0.31	11.35	± 0.37	Y
	5.0	35.30	± 0.45	35.29	± 0.51	Y	18.40	± 0.46	18.06	± 0.48	Y

Key for Tables 5 – 9

[p] Uncertainties estimated at 95 % Confidence Level by Monte Carlo Modelling. These do not include allowances for the finite size of flange and measuring vessel, nor the poor wettability for the water samples.

[q] Complex permittivity calculated at measurement temperature from the Debye parameters given in [36].

[r] Uncertainties are computed from uncertainties of the Debye parameters and measurement temperature uncertainty thereof given in [36], and also the sample temperature measurement uncertainty given in Column 1.

[s] Columns indicate whether for ε′ or ε″

$$\left|\text{Meas} - \text{Ref}\right| \le \sqrt{U_{\text{Meas}}^2 + U_{\text{Ref}}^2} \quad \text{(Yes/No)}.$$

The least-squares calibration procedure outlined in Section 4 was used for all of the sensors. Ethanol (reference liquid), open-circuit, and three short-circuit measurements were used. Short-circuits for the NPL sensors were obtained with foil as described in Section 5. For the Agilent sensor a plain metal short-circuit was used, considerable pressure being required to obtain small residual errors.

The effects of flange resonances are significant for the 15.1-mm coaxial sensor only (Table 7). At 1.0 GHz, the measured loss is greater than that expected for methanol on account of a flange resonance – given enough frequency points a low Q-factor resonance is evident on the VNA trace with centre frequency approximately 900 MHz. The measurements on DMSO also show very significant resonance effects, although none of the frequencies listed in Table 7 coincides with a resonant frequency (these occur at 0.8 and 1.2 GHz). The 15.1-mm sensor would not normally be used at frequencies above 500 MHz.

MCM was used to determine uncertainties. As can be seen (Tables 7-9) measurements and uncertainties are on the whole consistent, despite the shortcomings in the MCM that have already been discussed (Section 6). In any case, the confidence limits are expected to include only 95% of possible values that could be attributed to the measurand [58]. In a practical application, additional estimated allowances would be made for effects not considered in the MCM. It may be observed that the MCM estimates of uncertainties of the real and imaginary permittivity results obtained are closer to being equal in *absolute size* rather than as percentages, particularly at the lower frequencies.

7.4 Case study: Estimated uncertainties of measurements on tissue-equivalent material at Magnetic Resonance Imaging (MRI) frequencies

Exposure to RF radiation causes a temperature rise in the human body, which can be assessed by using body phantoms comprised of tissue-equivalent material [66]. In MRI systems, high-power fields in the frequency range 30 - 130 MHz are generated so there is a risk that hyperthermia may cause injury to patients. If a device has been implanted in a patient, whether permanently or during interventional MRI, localised heating may also be a hazard. A further issue is the occupational exposure of health workers, which will, in the future, be limited in Europe by the EU Physical Agents (Electromagnetic Fields) Directive [67]. Measurement of SAR and of temperature rises in the locality of implantable devices [68] requires the use of suitable TEMs, and hence requires complex permittivity measurements at MRI frequencies, e.g. at 43 MHz for a 1 Tesla machine. For solid materials and gels, large coaxial sensors are probably the most suitable instrument for this type of work. Discontinuous-inner-conductor coaxial reflection cells [69] [70] [71] can give smaller uncertainties at MRI frequencies, but are best suited to measurements on liquid samples.

Table 10: Uncertainties estimated by MCM of measurements on a uniform tissue-equivalent material at 50 MHz using 7-mm and 15.1-mm coaxial sensors. They are presented at coverage factor *k=2*, i.e. approx. 95% Confidence Level. The MCM is based on the uncertainty contributions listed in Table 2.

	Sample complex permittivity			
Sensor	**ε´**	**Unc.**	**ε´´**	**Unc.**
7-mm	77	± 7	244	± 5
15.1-mm		± 4		± 3

By using the Monte-Carlo Modelling process described in this paper, the uncertainties of measurements are estimated for 7-mm and 15.1-mm sensors for a uniform sample of tissue-equivalent material having complex permittivity $\varepsilon^* = 77 + j244$ at 50 MHz (Table 10). This is the complex permittivity of muscle at this frequency as given in [72]. As expected, the larger sensor enables measurement with smaller uncertainties. In practice, solid TEMs [66] are often gels that are far from ideal as specimens (e.g. they may be opaque materials that contain air bubbles) so additional uncertainty contributions may be needed. As a consequence of the low measurement frequency and the high loss of the sample, measurements can normally be expected to be unaffected by volumetric and flange resonances.

8. CONCLUSIONS

Various aspects of coaxial sensor metrology have been presented and reviewed, with special emphasis being placed upon traceability to international standards, the improvement of accuracy, and the estimation of measurement uncertainties. Measurements made with sensors of three different sizes have been presented. Among other observations, it has been shown experimentally that precision sensors can be calibrated at room temperature and used at temperatures up to 40 ºC without significant error due to the temperature change. This finding is relevant to *in vivo* biomedical measurements [7][32][73].

A least-squares method for calibration and a Monte-Carlo Modelling (MCM) method for estimating uncertainties have been described here in detail, and used to estimate the uncertainties of all of the measurements given. MCM enables uncertainties to be assessed in a more rigorous way than previously possible. The predicted uncertainties have been observed to be largely consistent with measurements made on reference liquids using the three sensors. The most significant aspect of this work is that it enables estimation of the uncertainties of samples for which comparable reference materials do not exist, e.g. measurement of tissue-equivalent materials at MRI frequencies. The impending implementation of the EU Physical Agents (Electromagnetic Fields) Directive in Europe [67] requires such measurements.

The MCM method described here does not cover the full measurement uncertainty (see Section 6). Simple

experiments can be performed to estimate additional allowances where appropriate (e.g. for boundary effects). Measurements on high surface-tension samples, e.g. water, can be improved if care is taken to remove bubbles (which may be too small to be visible easily), but even so it may be appropriate to make a small allowance for poor wettability (e.g. ~1% of real and imaginary parts of permittivity at $k=2$).

The estimated uncertainties of the measurements presented in this paper are quite low. Nevertheless it is still recommended that coaxial sensors are not used for obtaining reference data unless there is no better alternative. Methods such as transmission cells [71] that provide traceability directly to impedance standards and dimensions rather than a reference liquid are preferred.

ACKNOWLEDGMENTS

This work was undertaken in support of the UK National Measurement System (NMS) and was funded by the UK Department of Trade and Industry as part of its NMS Electrical Programme. The authors are grateful for the support of the following colleagues. G T Anthony, formerly of NPL, gave useful advice on least-squares fitting. T E Hodgetts of Qinetiq and A G P Warham, formerly of NPL, wrote the computer software that was used for calculating the reflection coefficient of coaxial sensors.

REFERENCES

[1] 2003 *IEEE recommended practice for determining the peak spatial-average specific absorption rate (SAR) in the human head due to wireless communications devices: Measurement techniques* IEEE Standard 1528-2003 ISBN 0-7381-3716-2

[2] 2001 *Basic standard for the measurement of specific absorption rate related to human exposure to electromagnetic fields from mobile phones (300 MHz - 3 GHz)* CENELEC standard EN 50361:2001,

[3] 2005 *Human exposure to radio frequency fields from hand-held and body-mounted wireless communication devices - Human models, instrumentation, and procedures - Part 1: Procedure to determine the specific absorption rate (SAR) for hand-held devices used in close proximity to the ear (frequency range of 300 MHz to 3 GHz),* IEC Standard 62209-1

[4] Gregory A P, Clarke R N, Hodgetts T E and G T Symm 1993 *RF and Microwave dielectric measurements using a reflectometric coaxial sensor*, NPL Report DES 125 ISSN 0143-7305

[5] Gregory A P and Clarke R N 2006 A Review of RF and microwave techniques for dielectric measurements on polar liquids *IEEE Trans. Dielectrics and Electrical Insulation* **13 (**4) 727-743

[6] Neubauer H and Huber F R 1969 Higher modes in coaxial RF lines *Microwave Journal* **12** (6) 57-66

[7] Grant J P, Clarke R N, Symm G T and Spyrou N M 1988 *In vivo* dielectric properties of human skin from 50 MHz to 2.0 GHz *Phys. Med. Biol.* **33**, (5) 607-612

[8] Hodgetts T E 1981 *The calculation of the equivalent circuits of coaxial-line step discontinuities*, Royal Signals and Radar Establishment Memorandum No. 3442, UK

[9] Fuks R New Dielectric 2001 Bead For Millimetre-Wave Coaxial Components *Microwave Journal* **44** (5) 318

[10] Williams B 2004 *Over Moding Transmisssion Characteristics of Type-N Connector 7-mm line between 18 and 26.5 GHz* ANAMET report No. 44 National Physical Laboratory, UK

[11] Somlo P I 1967 The Computation of Coaxial Line Step Capacitances *IEEE Trans. Microw. Theory Tech.* **MTT-15 (**1) 48-53

[12] Whinnery J R and Jamieson H W 1944 Equivalent circuits for discontinuities in transmission lines *Proc. IRE* **32** 98-114

[13] Okoniewski M, Anderson J, Okoniewska E, Caputa K and Stuchly S S 1995 Further analysis of open-ended dielectric sensors *IEEE Trans. Microw. Theory Tech.* **MTT-43** (8) 1986-89

[14] Evans S 1997 The shielded open-circuit probe for dielectric measurements *Proceedings of The British Electromagnetic Measurements Conference* BEMC 1997

[15] Olmi R and Bini M 2004 Improvement of the permittivity measurement by a 3D full-wave analysis of a finite flanged coaxial probe *J. of Electromagn. Waves and Appl.* **18** (2) 217-232

[16] Yu-Sun J, Se-Yun K 2004 FDTD Validation on an improved virtual transmission line conversion model of open-ended coaxial probe *IEEE Antennas and Propagation Society Symposium* **4** 4543-4546

[17] Hoshina S, Kanai Y and Miyakawa M 2001 A Numerical Study on the Measurement Region of an Open-Ended Coaxial Probe Used for Complex Permittivity Measurement *IEEE Trans. Magnetics* **37** (5) 3311-3314

[18] Hagl D M, Popovic D, Hagness S C, Booske J H and Okoniewski M 2003 Sensing Volume of Open-Ended Coaxial Probes for Dielectric Characterisation of Breast Tissue at Microwave Frequencies *IEEE Trans. Microw. Theory Tech.* **MTT-51** (4) 1194-1206

[19] Hodgetts T E 1989 *The open-ended coaxial line: a rigorous variational treatment*, Royal Signals and Radar Establishment Memorandum No. 4331, UK

[20] Warham A G P 1989 *Annular slot antenna radiating into lossy material* National Physical Laboratory Report DITC 152/89

[21] Nevels R D, Butler C M and Yablon W 1985 The annular slot antenna in a lossy biological medium *IEEE Trans. Microw. Theory Tech*. **MTT-33** (4) 314-319

[22] Mosig J R, Besson J E, Gex-Fabry M and Gardiol F E 1981 Reflection of an open-ended coaxial line and application to nondestructive measurement of materials *IEEE Trans. Instrum. Meas*. **IM-30** (1) 46-51

[23] Pournaropoulos C L and Misra D 1994 A study on the coaxial aperture electromagnetic sensor and its application in material characterisation *Trans. IEEE Trans. Instrum. Meas.* **IM-43** (2) 111-115

[24] Asvestas J S 2006 Radiation of a Coaxial Line Into Half-Space *IEEE Trans. Ant.. and Propag.* **AP-54** (6) 1624-1631

[25] van Damme S, Franchois A, de Zutter D and Taerwe L 2004 Nondestructive determination of the steel fiber content in concrete slabs with an open-ended coaxial probe *IEEE Trans. on GeoScience and Remote Sensing*, **42** (11 2511-2521

[26] Pournaropoulos C L and Misra D K 1997 The co-axial aperture electromagnetic sensor and its application in material characterization *Meas. Sci. Technol.* **8** (11) 1191-1202

[27] Blackham D V and Pollard R D 1997 An improved technique for permittivity measurements using a coaxial probe *IEEE Trans. Instrum. Meas.* **IM-46** (5) 1093-1099

[28] Jenkins S, Hodgetts T E, Symm G T, Warham A G P, Clarke R N and Preece A W 1990 Comparison of three numerical treatments for the open-ended coaxial line sensor *IEE Elect. Lett*. **26** (4) 234-235

[29] Kraszewski A, Stuchly M A and Stuchly S S 1983 ANA calibration method for measurements of dielectric properties *IEEE Trans. Instrum. Meas.* **IM-32** (2) 385-387

[30] C Gabriel, T Y A Chan and E H Grant 1994 Admittance models for open ended coaxial probes and their place in dielectric spectroscopy *Phys. Med. Biol.* **39 (**12) 2183-2200

[31] Otto G P and Chew W C 1991 Improved Calibration of a Large Open-Ended Coaxial Probe for Dielectric Measurements *IEEE Trans. Instrum. Meas.* **IM- 40** (4) 742-746

[32] Popovic D, McCartney L, Beasley C, Lazenik M, Okoniewski M, Hagness S C, Booske J H 2005 Precision open-ended coaxial probes for in vivo and ex vivo Spectroscopy of biological tissues at microwave frequencies *IEEE Trans. Microw. Theory Tech.* **MTT-53** (5) 1713-1721

[33] Huynh J and Augustin D 2004 Advances in Probe Development and Calibration Procedure Enhance Material Measurements *IEEE Conf. on Infrared and Millimetre Waves and Terahertz Electronics (Karlsruhe)*, 215-216

[34] Clarke R N (Ed.) 2003 *A Guide to the characterisation of dielectric materials at RF and microwave Frequencies* The Institute of Measurement and Control (IMC) and The National Physical Laboratory (NPL), London, ISBN 0 904457 38 9

[35] Williams G and Thomas D K 1998 *Phenomenological and molecular theories of dielectric and electrical relaxation of materials* Novocontrol Applications Note - Dielectrics NR.3

[36] Gregory A P and Clarke R N 2001 *Tables of the Complex Permittivity of Dielectric Reference Liquids at Frequencies up to 5 GHz* NPL Report CETM 33, ISSN 1467-3932

[37] Sato T, Chiba A and Nozaki R 1999 Dynamical aspects of mixing schemes in ethanol-water mixtures in terms of the excess partial molar activation free energy, enthalpy and entropy of the dielectric relaxation process *J.Chem. Phys*. **110** (5) 2508-2521

[38] Petong P, Pottel R, and Kaatze U 1999 Dielectric relaxation of H-bonded liquids, mixtures of ethanol, and n-hexanol at different temperatures and compositions *J. Phys. Chem.* **103** 6114-6121

[39] Sato T, Chiba A and Nozaki R 2000 Hydrophobic hydration and molecular association in methanol-water mixtures studied by microwave dielectric analysis *J.Chem. Phys.* 112 (6) 2924-2932

[40] Kaatze U 1989 Complex permittivity of water as a function of frequency and temperature *J. Chem. Eng. Data* **34** (4) 371-374

[41] Hamelin J, Mehl J B and Moldover M R 1998 Resonators for accurate dielectric measurements in conducting liquids *Rev. Sci. Instrum*, **69 (**1) 255-260

[42] Lamkaouchi K, Balana A, Delbos G and Ellison W J 2003 Permittivity measurements of lossy liquids in the range 26-110 GHz *Meas. Sci. Tech.* **14** (4) 444-450

[43] Vij J K , Grochulski T , Kocot A and Hufnagel F 1991 Complex permittivity measurements of acetone in the frequency range 50-310 GHz *Molecular Physics* **72** (2) 353-361

[44] Stogryn A 1971 Equations for calculating the dielectric constant of saline water *IEEE Trans. Microw. Theory Tech.* **MTT-19** (8) 733-736

[45] Nortemann K, Hilland J and Kaatze U 1997 Dielectric properties of aqueous NaCl Solutions at microwave frequencies *J. Phys. Chem. A* **101** 6864-6869

[46] Buchner R, Hefter G T, and May P M 1999 Dielectric relaxation of aqueous NaCl solutions *J. Chem. Phys. A* **103** 1-9

[47] T Chen, G Hefter and R Buchner 2003 Dielectric spectroscopy of aqueous solutions of KCl and CsCl, J Chem. Phys. A, **107** 4025-4031

[48] Davey C L and Kell D B 1998 The influence of electrode polarisation on dielectric spectra, with special reference to capacitive biomass measurements I. Quantifying the effects on electrode polarisation of factors likely to occur during fermentations *Bioelectrochemistry and Bioenergetics* **46** 91-103

[49] Gregory A P and Clarke R N 2005 Traceable Measurements of the Static Permittivity of Dielectric Reference Liquids over the Temperature Range 5 - 50 °C *Meas. Sci. Technol.* **16** (7) 1506-1516

[50] Fitzpatrick J 1978 Error models for systems measurement *Microwave Journal* **21** (5) 63-66

[51] Bianco B, Corana A, Ridella S, Simicich C 1978 Evualation of Errors in Calibration Procedures for Measurements of Reflection Coefficient *IEEE Trans. Instrum. Meas.* **IM-27** (4) 354-358

[52] Evans S and Michelson S C 1995 Intercomparison of dielectric reference materials available for the calibration of an open-ended probe at different temperatures *Meas. Sci. Tech*. **6** (12) 1721-1732

[53] Salter M J, Ridler N M and Harris P M 2003 Over-determined calibration schemes for RF network analysers employing generalized distance regression, *62nd ARFTG Microwave Measurements Conference*, 127-142

[54] *The NAG Fortran 77 Library, Mark 20* NAG Ltd Wilkinson House, Jordan Hill Road, Oxford, 2001

[55] Cox M G, Dainton M P and Harris P 2001 *Software support for metrology best practice guide no.6: Uncertainty and statistical modelling* NPL Report, ISSN 1471-4124

[56] Hall B D 2006 Monte Carlo uncertainty calculations with small-sample estimates of complex quantities *Metrologia*, **43** (3) 220-226

[57] Cox M G and Siebert B R L 2006 The use of a Monte Carlo method for evaluating uncertainty and expanded uncertainty *Metrologia* **43** (4) 178-188

[58] BIPM, IEC, IFCC, ILAC, ISO, IUPAC, IUPAP, and OIML Evaluation of measurement data – Supplement 1 to the "Guide to the expression of uncertainty in measurement" - Propagation of distributions using a Monte Carlo method, in preparation (publication due 2007). Joint Committee for Guides in Metrology, Bureau International des Poids et Mesures.

[59] Gregory A P and Clarke R N 2006 Monte-Carlo Simulation Of The Uncertainties Of Coaxial Sensor Dielectric Measurements *Proceedings of the Conference on Precision Electromagnetic Measurements* **CPEM 2006**

[60] Popovic B and Okoniewski M 2002 Effects of mechanical flaws in open-ended coaxial probes for dielectric spectroscopy, *IEEE Microw. and Wireless Components Lett*. **12** (10) 401-403.

[61] Colpitts B G 1993 Temperature Sensitivity of Coaxial Probe Complex Permittivity Measurements: Experimental Approach *IEEE Microw. Theory Tech.* **MTT-41** (2) 229-233

[62] Riddle B, Baker-Jarvis J and Krupka J 2003 Complex permittivity Measurements of Common Plastics Over Variable Temperatures *IEEE MTT*, **51** (3) 727-733

[63] Arai M, Binner J G P and Cross T E 1995 Correction of errors owing to thermal elongation of high temperature coaxial probe for microwave permittivity measurement *Electr. Lett.,* **31** (14) 1138-1139

[64] Bringhurst S and Iskander M F 1996 Open-ended metallized ceramic coaxial probe for high-temperature dielectric properties measurements *IEEE Trans. Microw. Theory Tech.* **MTT-44** (6) 926-935

[65] 1995 *Guide to the Expression of Uncertainty in Measurement* (Geneva: International Organisation for Standardization)

[66] Chou C-K, Chen G-W, Guy A W and Luk K H 1984 Formulas for Preparing Phantom Muscle Tissue at Various Radiofrequencies *Bioelectromagnetics*, **5** (4) p435-441

[67] Directive 2004/40/EC of the European Parliament and of the Council of 29 April 2004 on the minimum health and safety requirements regarding the exposure of workers to the risks arising from physical agents (electromagnetic fields) (18th individual Directive within the meaning of Article 16(1) of Directive 89/391/EEC) 2004 *Official Journal* **L 159** (2004) 1-26, Corrigendum **L 184** (2004) 1-9

[68] *Standard Test Method for Measurement of Radio Frequency Induced Heating Near Passive Implants During Magnetic Resonance Imaging* ASTM Standard F2182-02a

[69] Jenkins S, Hodgetts T E, Clarke R N and Preece A W 1990 Dielectric measurements on reference liquids using automatic network analysers and calculable geometries *Meas. Sci. Tech.* **1** (8) 691-702

[70] Gottmann O, Kaatze U and Petong P 1996 Coaxial to circular waveguide transition as high precision easy-to-handle measuring cell for broad band dielectric spectrometry of liquids *Meas. Sci. Tech.* **7** 525-534

[71] Gregory A P and Clarke R N 2002 Traceable measurements on dielectric reference liquids over the temperature range 10-50 ºC using coaxial line methods *Proceedings of the Conference on Precision Electromagnetic Measurements* CPEM 2002

[72] Gabriel C 1996 *Compilation of the Dielectric Properties of Body Tissues at RF and Microwave Frequencies*, Brooks Air Force Technical Report AL/OE-TR-1996-0037

See http://www.fcc.gov/cgi-bin/dielec.sh

[73] Nuutinen J, Ikaheimo R and Lahtinen T 2004 Validation of a new dielectric device to assess changes of tissue water in skin and subcutaneous fat *Physiol. Meas*. **25** 447-454